CREEP FRACTURE IN HASTELLOY XR

K. KIKUCHI
JAERI, Tokai-mura, Ibarak-ken, Japan

I.J. O'DONNELL
UKAEA, Risley, Warrington, England

ABSTRACT

Hastelloy XR will be used as tubing material in the intermediate heat exchangers of the High Temperature gas-cooled Reactor(HTR), and will be subjected to operating temperatures in the range of 800°C to 950°C. Creep behaviour in tension has been characterized on Hastelloy XR, and the creep damage micromechanisms of void nucleation, growth and interlinkage have been studied in-situ using scanning electron microscopy. Intergranular creep failure was observed, and the rates of damage at grain boundaries were determined. The effects of applied stress, strain rate and constraint (through the effect of surface proximity) on creep damage development are discussed with reference to model behaviour. The results indicate a significant surface effect on creep deformation behaviour and fracture micromechanisms.

1. INTRODUCTION

Hastelloy XR is a nickel based alloy and will be used as tubing material in the intermediate heat exchangers of the High Temperature gas-cooled Reactor(HTR). In normal operation it will be subjected to stresses of approximately a couple of ten MPa and temperatures in the range of 800° to 950°C, but it may experience higher stress levels under transient conditions. The objective of this project is to characterize the creep fracture behaviour of Hastelloy XR, with particular emphasis on the identification of the failure micromechanisms and their controlling parameters. Although methods exist for assessing creep life times, by the empirical Monkman-Grant product for example, in which the product of the steady state creep rate and the time to rupture is approximately constant, it is not fully clear why these estimation techniques work. A fundamental study of the fracture mechanisms has been undertaken, so that estimation techniques may be underpinned experimentally. In the first part of this report some of the basic models describing creep deformation and fracture are outlined. Secondly, the results obtained within the course of this work are presented, and finally these are compared with some of the model based predictions of creep behaviour (particularly with regard to void growth in creep).

2. CREEP DEFORMATION AND FRACTURE

Mechanistically creep deformation has been described by theories involving dislocation glide and climb past obstacles on the slip plane - *dislocation creep*, by diffusive flow of matter along grain boundaries - *Coble creep*, or by diffusive flow through the bulk crystal - *Herring-Nabarro creep*. The favoured mechanism depends critically on stress, temperature and the grain boundary and bulk diffusion coefficients. The equations describing these creep processes are given in Appendix I. A map of creep deformation mechanism has been constructed using the data for pure Nickel given in reference (1), and this is shown in Fig 1. The map shows that dislocation creep is favoured by large grain sizes, high stress and high temperature. Improving the creep resistance of a material is usually achieved by additional alloying, which impedes dislocation activity, the result being to enlarge the Coble creep regime. With reference to service applications, the appropriate creep regime should be studied to ensure applicability of the data to the component. Generally speaking the Herring-Nabarro regime only occurs at very high temperatures and low stresses, and is not significant in electrical generating plant.

Many experimental observations have shown that fracture in either the dislocation (power law) creep or Coble regime is characterized by intergranular failure, caused by coalescence of voids nucleated on grain boundaries. In simple tension grain boundaries, orientated with a plane normal approximately coincident with the stress axis, show preferential void formation compared with boundaries significantly inclined to the stress axis. Nucleation can occur homogeneously at the grain boundary or at the interface of a precipitate located on the boundary. The mechanisms controlling nucleation are not fully resolved. However, several important features have been identified, and these include: stress concentrations caused by slip lines at grain boundaries, stress concentrations produced by grain boundary sliding, precipitate interfacial energy effects and the effect

of segregation on the cohesive strength of boundaries or precipitate-boundary interfaces. Importantly, even in the dislocation creep regime where deformation rate is controlled by bulk diffusive effects, the fracture mechanism is controlled by grain boundary behaviour.

The applied stress produces vacancy enrichment close to the normal boundaries, and once nucleated a void will grow by vacancy adsorption if the applied stress is greater than the sintering stress, which is typically 2-4MPa. Material will be plated out from the voids and the specimen will strain. Several theories have been developed to explain the growth of intergranular voids by grain boundary diffusive mechanisms. Fig 2 shows schematically the situation in a creeping polycrystal subjected to a remote tensile stress, σ_∞. In the original model due to Hull and Rimmer [2] the local stress on the normal boundaries, σ_b, is assumed to be equal to the remote stress, and inclined boundaries are assumed to slide easily. In this unconstrained regime; the growth rate in terms of the void radius, a, is given by

$$\dot{a} = \frac{2\Omega\partial D_b\{\sigma_\infty - \sigma_e(1-f)\}}{kTh(\Psi)a^2 q(f)} \qquad \ldots.1$$

The terms are defined in Appendix I, and $q(f) = [2\ln\frac{1}{f} - (3-f)(1-f)]$. Usually however, the predictions of void growth rates based on this model, have been found to be too high.

Dyson[3] considered that in polycrystalline structure constraints on the movement of the grains would occur, either as a result of impaired sliding or because the voided boundaries were inhomogeneously distributed in the material. The effect of these constraints would be to attenuate the stress on the normal boundaries; the normal boundaries would shed load to the inclined boundaries so that the actual local tensile stress at the normal boundaries $\sigma_b < \sigma_\infty$. Rice[4] developed the model and showed that, if the deformation was constrained in this way, cavity growth rates would be significantly reduced. Indeed, whilst the voids grow by a diffusive mechanism the overall deformation is controlled by dislocation glide and climb mechanisms with a remote strain rate $\dot{\varepsilon}_\infty$. According to Rice cavity growth rate in the constrained regime is given by

$$\dot{a} = \frac{\alpha b^2 d\dot{\varepsilon}_\infty}{4h(\Psi)a^2}\{1-(1-f)\frac{\sigma_a}{\sigma_\infty}\} \qquad \ldots.2$$

where α is constant approximately equal to 1.8 in power law creeping materials, and d is the boundary diameter. Calculations based on these models are compared with the experimental results later. Also it was shown, from purely diffusion and deformation considerations, that a diffusion path length parameter, L, can be defined which characterizes whether or not constrained or unconstrained growth may be expected. L is given by

$$L = \left(\frac{\Omega\partial D_b\sigma_\infty}{kT\dot{\varepsilon}_\infty}\right)^{1/3} \qquad \ldots.3$$

Below a particular stress level the diffusion path length is greater than the cavity half spacing, and the strain can be supplied entirely by the plating out of atoms from the voids. At higher stress levels the path length is less than the cavity half spacing, and some deformation of the grains by power law creep must occur; growth is thereby unconstrained. In nickel a stress below approximately 100MPa would be required for constrained growth at 800°C if the cavity half spacing is approximately 1μm (a typical value).

Rice showed that integration of Equation 2 would lead to a Monkman-Grant dependency for coalescence of voids on a boundary, whereas this is not the case for Equation 1. Importantly the concept of geometric constraint was extended further by Anderson and Rice [5] who considered the deformation requirements in a 3-dimensional polycrystal. One aspect of the results showed that whilst in a two-dimensional system, such as that shown in Fig 2, it is possible to produce strain by rigid body movements of the grains by sliding, in 3-D, the bulk of the grains must also deform to retain contiguity across the inclined boundaries. Therefore, even with free sliding, and a homogeneous distribution of voided grain boundaries, power law creep is required to maintain deformation compatibility[7].

The progression from void nuclei through to a grain boundary microcrack has been outlined. However, the failure of a grain boundary facet constitutes only a lower bound condition for the failure of a specimen in general, since additional strain is often required to interlink these micro-cracks. Generally this strain is found by experiment to be significant. In numerical FE analysis Tvergaard[6] has also shown that this strain is expected to be large (40-80 %). For the Monkman-Grant correlation to work successfully damage processes in different creep regimes must occur with approximately similar kinetics. However, this may not be expected since the crack interlinkage regime is associated with the tertiary creep stage, in which the strain rate is much higher than in the secondary creep regime.

3. EXPERIMENTAL DETAILS

Material

The composition of Hastelloy XR is given in Table 1. It is a nickel based super alloy that has been specially developed to have a high oxidation resistance and good high temperature mechanical properties in power plant environment. The material is used in the solution treated condition, and here it has been heat treated for 1h at 1149°C.

Creep testing

Creep specimens of dimensions shown in Fig 3 were machined from 2mm thick plate. The specimens were loaded in uniaxial tension using a servo-hydraulic test machine with a horizontal load string. The portion containing the specimen and grips was located inside the chamber of a SEM, operating at a pressure of approximately 10^{-6}Pa. Three creep tests were performed at a temperature of 800°C with applied stresses of 60, 80 and 110MPa.

Because of space limitations in the microscope chamber it was not possible to fit external extensometer on to a specimen. Initially, a grid was marked on a specimen using a microhardness machine, and strains were measured from photographs of the grid. In the latter tests a direct measurement system was used, in which the whole actuator was moved to determine the displacement between two points marked on the specimen surface. This latter technique gives a measuring accuracy of ± 0.001(ε). Within the course of this work significant advances in the imaging quality of the system have been made, principally by reducing the transmission of vibrations to the actuator arm.

Creep damage assessment

Creep damage was followed on the specimen surface in the SEM. In order to ensure observations were made on damage free surfaces, the gauge length of the specimens was electro-polished prior to testing, using Struers A2 sol[8] at 10V. A systematic technique for assessing damage was employed, in which a specific area was repeatedly studied throughout the creep test. A rectangular box 1mm x 0.4mm was engraved on the specimen. A montage of photographs at 500x magnification was taken of the enclosed area at intervals throughout the test. The grain boundaries within the boxed area were classified into normal or inclined boundaries (for the latter the plane normal >30° from principal stress axis). Each boundary was then studied to detect (i) if void nucleation had occurred on any part of the boundary, (ii) had all the voids nucleated, i.e.,. was the boundary fully voided and (iii) had the voids on the boundary coalesced. The number fraction of damaged boundaries was then determined and can be expressed as a function of time, strain or life fraction (based on rupture time or ductility). The growth rate of individual cavities was determined by measurements from photographs taken at 2000x magnification. Grain deformations at and under surface was assessed from the photographs, and by sectioning and metallographically preparing the specimens after fracture, respectively.

4. RESULTS

Microstructural development in creep tests at 800 °C

In the solution treated condition the structure consists of a heavily twinned austenitic matrix. The grain size is not uniform and varies from 50μm up to approximately 400μm. Heavy precipitation occurs at 800°C even in short term creep tests. Coarse particles of sizes around 1μm form on the grain boundaries, somewhat smaller particles but of a similar morphology form on the twin boundaries, and fine precipitation occurs within the grains. According to TEM observations the coarse particles were found to be Mo, Ni and Cr rich, and are therefore most likely to be M_6C. The fine particles were predominantly

Cr rich and are most probably $M_{23}C_6$. Both of these phases are commonly found in nickel based super alloys.

Creep damage assessment

Creep curves obtained from the three tests are shown in Fig 4. The time to fracture, t_f, rupture strain, ε_f, and minimum creep rate, $\dot{\varepsilon}_\infty$, are summarized in Table 2. A least squares linear fit to the log stress vs. log $\dot{\varepsilon}_\infty$ data gives a creep exponent, n, of approximately 4. Plots of grain boundary creep damage vs. strain are shown in Figs 5a to 5f. In all of the tests, comparing results obtained on normal or inclined boundaries shows that, as expected, the normal boundaries cavitate and coalesce more rapidly than the inclined boundaries. When plotted as a function of strain it is seen, at stresses of 60 and 80MPa, that normal boundaries become fully voided at strains of less than 2%. However, at 110MPa void nucleation is protracted, with only approximately half the boundaries fully voided at that strain. Likewise, the inclined boundaries damage at significantly slower rate, with respect to strain, at the highest stress level.

Fig.6 shows examples of void development at a stress of 80MPa. The voids identified in the figure were measured at successive intervals during secondary creep, and Figs 7a and b show plots of void radius in the transverse and tensile directions as a function of time. The void growth rate, with the exception of the transverse growth rate for void 1, was in the range 1 to 2 $\times 10^{-12}$ m / s. The lower transverse growth rate for void 1 may be attributable to the inhibiting effect of the precipitate located equatorially on the right hand side of the void. Void growth rates were measured in the other tests and plots of log growth rate vs. log stress are shown in Figs.8a and 8b for growth in the transverse and tensile directions respectively. In each case the gradient is around unity.

Qualitatively the assessment of grain deformation showed that at 60 and 80MPa the surface grains behaved essentially in a rigid manner and did not change shape throughout the creep test. At 110 MPa the surface grains were heavily deformed during creep as shown in Fig.9. Grain size for tensile direction was measured at the same grains where growth of voids was observed. The bulk behaviour at 60 and 80 MPa was non rigid and similar to that at 110MPa.

5. DISCUSSION

Creep damage has been quantitatively measured in a series of tests at 800°C over a stress range of 60 to 110MPa. The results indicate that the grain boundary damage (with respect to strain) is a function of the applied stress. Observations of grain deformation have shown that at 60MPa and 80MPa the grains at the specimen surface behave essentially like rigid blocks. In Fig.9 measurements of individual grains show that no significant grain deformation is occurring, therefore, the strain at the surface is supplied by diffusional void growth at the grain boundaries, accommodated presumably by grain boundary sliding. However, sectioned and polished specimens show that bulk deformation of the grains does occur below the surface, and of course, the measurement of a creep exponent of 4 shows dislocation controlled creep behaviour. Therefore, grain behaviour internally is of a 3-D nature as described by Anderson and Rice, whilst that of the surface grains is essentially 2-D. The strain rate at the surface must equal that of the internal grains, and so the behaviour of the surface is analogous to the constrained growth regime described by Dyson and Rice, with void growth occurring by diffusion, but at a rate controlled by bulk deformation creep. Satisfaction of the strain requirement almost entirely by diffusive void growth means that, compared with the internal boundaries, the grain boundaries at the surface fail earlier and at lower strains. It seems apparent that in this regime of behaviour surface microcracks will form if strain in the material exceeds 1-2%. Indeed, because the grains are behaving more rigidly, it appears that the strain requirement is reduced as the stress falls, and more deformation is concentrated at the grain boundaries.

At the highest stress level (110MPa) significant bulk deformation of the surface grains is observed. It is assumed that the diffusion length parameter, L, calculated for nickel can be approximately applied to Hastelloy XR. On this basis and noting that the inter-void half spacing, b, is approximately 1μm, then for a stress of 110MPa, L is slightly less than b. In those circumstances even the surface grains must deform by power law creep to maintain the strain rate. That is to say, constrained growth is not occurring because of the

strain rate requirements, rather than a geometrically induced constraint effect of the type described earlier. The effect that this produces with reference to the damage rate at the grain boundaries is very interesting, not only is the damage at the normal grain boundaries reduced, but perhaps more significantly the damage at the inclined boundaries is even more severely retarded with respect to strain. Generally, in sectioned creep test specimens tested at low or high stresses it is frequently seen that, even at failure, relatively few inclined boundaries are severely damaged. The reduction in damage may be associated with the occurrence of power law creep at both low stresses (where it occurs in the bulk of the specimen below the surface grains) or at high stresses both internally and at the surface. The observed retardation of damage may be a consequence of reduced sliding of the inclined boundaries in the dislocation creep regime. Void nucleation by sliding may be reduced, or since the local shear stresses are not relaxed if sliding is reduced, then local normal tensile stresses near the boundary are low, and the possibility for void growth is also retarded.

In the context of this work, that the surface behaves in a different manner from the internal structure (at low stresses in particular) is a significant finding. There is clear evidence that, if the bulk were to damage at the same rate as the surface, much lower failure time and ductility would result. It is not clear yet if the behaviour of the material at the lower stress levels is dominated by the growth of the surface cracks through the net section, or if bulk damage becomes the critical parameter in determining creep life. It is, however, likely that thin walled components will be more susceptible to the effects of surface microcracking than thick walled plant.

The void growth rate results from the measurements of individual voids show a large variation. In a pseudo constrained regime (the surface is displaying unconstrained features but the strain rate is controlled by bulk behaviour) the relationship between log stress and log cavity growth rate for transverse direction should be linear with a gradient of n. The results here do not display that behaviour and the gradient of the curves in Fig.8 is closer to unity. That result would be expected for unconstrained growth of the Hull-Rimmer type, however, if Equation 1 is integrated (ignoring the sintering stress) then the time for growth of voids up to typical sizes observed here can be calculated. Results based on Equation 5 (where a_2 and a_1 are the final and initial void sizes) show that void growth would be expected to occur in minutes rather than the tens of hours observed.

$$t_g = \frac{hkT}{2\partial D_b \Omega \sigma_\infty}\left(-\frac{2a^3}{3}\ln\frac{a^2}{b^2} - \frac{5a^3}{9} + \frac{4a^5}{5b^2} - \frac{a^7}{7b^4}\right)_{a_1}^{a_2} \qquad \text{....5}$$

The Hull Rimmer model is not therefore appropriate in this case. Integration of Equation 2 will give growth times for the constrained regime examined by Rice.

$$t_g = \frac{4h}{3\dot{\varepsilon}\alpha d b^2}(a_2^{\,3} - a_1^{\,3}) \qquad \text{....6}$$

Results based on equation 6 show that the predictions are close to the measured values at 60MPa whereas at 110MPa measured growth is slower than expected significantly. That is, t_g is calculated to be 510h, 123h and 37h for h=0.6, α=1.8, $d = 50\mu m$, $a_2 = 1.2\mu m$ and $a_1 = 0\mu m$ at σ=60, 80 and 110MPa, whereas voids begin to coalesce on normal grain boundaries at 500h, 180h and 110h, respectively.

6. SUMMARY

Creep tests were performed in the chamber of the SEM at high temperature and systematic techniques were developed for application to creep fracture micromechanism. The void development along the grain boundaries at surface and surface grain deformation were observed and then those were compared with bulk deformation to find surface effects on creep deformation and the creep micromechanism. The grain boundaries of Hastelloy XR were classified into normal or inclined boundaries to the remote stress axis and parameters were introduced to detect if void nucleation had occurred on the grain boundaries, had all the voids nucleated and had the voids coalesced. The followings are the summary of this work:

(1) The normal boundaries cavitate and coalesce more rapidly than the inclined boundaries. The grain boundary damage is a function of applied stress.

(2) The gradient of log growth rate of void versus log stress shows a large scattering but around unity statistically.

(3) The surface grain behaves in a different manner from the internal structure at low stresses: the behaviour of the surface is analogous to the constrained growth regime with void growth occurring by diffusion but at a rate controlled by bulk deformation. At high stress constrained growth doesn't occur and the damage at the inclined boundaries is severely retarded with respect to strain.

7. REFERENCES

1. Riedel H., Fracture at High Temperatures, ed. Ilschner and Grant, Springer-Verlag,Heidelberg 1987.
2. Hull D. and Rimmer D.E., Phil. Mag., **4**, 673, 1959.
3. Dyson B.F., Metal Sci., **10**, 349, 1976.
4. Rice J.R., Acta metall., **29**, 675, 1981.
5. Anderson P. M. and Rice J. R., Acta metall., **33**, 409, 1985.
6. Tvergaard V., Int. Jnl. Solids Structures, **21**, 279, 1985.
7. Raj R. and Ghosh A.K., Met. Trans. **12A**, 1291,.1981.

APPENDIX 1

The data given in Reference 1 used to construct the creep deformation map shown in Fig 1. The basic equations describing creep deformation are given below. The boundaries between the regimes are found by equating the strain rates.

In the **dislocation** creep regime Norton's law is obeyed and the strain rate is given by

$$\dot{\varepsilon} = B\sigma^n \qquad \ldots A1$$

where

$$B = A^* G^{1-n} (b_v D_v/kT) \qquad \ldots A2$$

and

$$D_v = D_{vo} \exp(-Q_v/RT) \qquad \ldots A3$$

in the **Coble** creep regime the strain rate is given by

$$\dot{\varepsilon} = \alpha_b \sigma \Omega \partial D_b/(kTd^3) \qquad \ldots A4$$

where

$$\partial Db = \partial D_{bo} \exp(-Q_b/RT) \qquad \ldots A5$$

and in the **Herring-Nabarro** creep regime the strain rate is given by

$$\dot{\varepsilon} = \alpha_v \sigma \Omega D_v/(kTd^2) \qquad \ldots A6$$

The meaning of the symbols and the values used here are given below. The deformation map is not normalized in the usual way (by melting temperature and shear modulus), so that a comparison with operating conditions can be made more easily.

$\dot{\varepsilon}$	strain rate	s^{-1}
B	constant in Norton's law	$Pa^{-n}s^{-1}$
σ	stress	Pa
n	creep exponent	5
A*	constant in Norton's law	3×10^6
G	shear modulus	79-0.032(T-9.6) GPa
b_v	Burgers vector	2.49×10^{-10} m
D_v	bulk diffusion coefficient	m^2s^{-1}
Q_v	activation energy for bulk diff.	284 kJmol^{-1}
D_{vo}	Pre-exponential factor	1.9×10^{-4} m^{2}s^{-1}
k	Boltzmann's constant	1.38×10^{-23} JK^{-1}
R	Gas constant	8.3 Jmol^{-1}K^{-1}
d	grain size (or facet size)	m
T	absolute temperature	K
∂D_b	grain boundary diffusion coeff.	m^3 s^{-1}
∂D_{bo}	Pre-exponential factor	$3.5 \times 10^{-15} m^3s^{-1}$
Q_b	activation energy for g.b. diff.	115 kJmol^{-1}
Ω	atomic volume	1.09×10^{-29} m^3
α_b	constant in Coble creep rate eqn.	50
α_v	constant in H-N creep rate eqn.	24
∞	*sub-script* remote value of	
σ_n	sintering stress	
a	void radius	
b	Cavity half spacing	
f	void volume fraction	a^2/b^2

α	constant dependent on gb sliding	1.8
$h(\psi)$	constant dependent on void shape $[1/\sin^3\psi][1-1.5\cos\psi+0.5\cos3\psi]$	0.6, ψ =70°

Table 1 Composition specification for Hastelloy XR(wt%).

C	Mn	Si	P	S	Cr	Co	Mo	W	Fe	B	Ni	Al	Ti
0.05	0.6	0.3	LAP	LAP	20.50	LAP	8.00	0.20	17.00	LAP	BAL	LAP	LAP
0.15	1.0	0.5	0.040	0.030	23.00	0.5	10.00	1.00	20.00	0.01	BAL	0.10	0.03

LAP: Low as possible

Table 2 Summary of creep test data.

Test No.	Stress (MPa)	Failure Time (h)	Failure Strain (%)	Minimum Creep Rate (1/h)
TEST 1	80	324	15	8.7×10^{-5}
TEST 2	60	1117	9	2.1×10^{-5}
TEST 3	110	203	17	2.0×10^{-4}

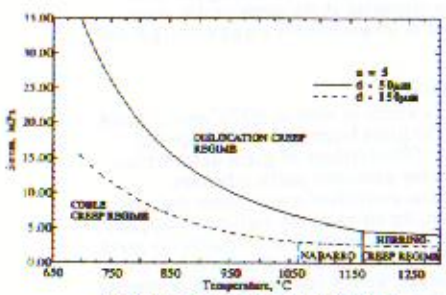

Fig.1 Creep deformation map for Nickel.

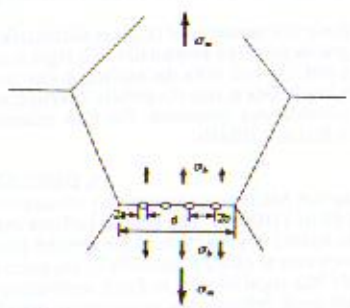

Fig.2 Schematic illustration of intergranular void growth.

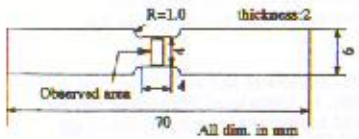

Fig.3 Creep test specimen geometry.

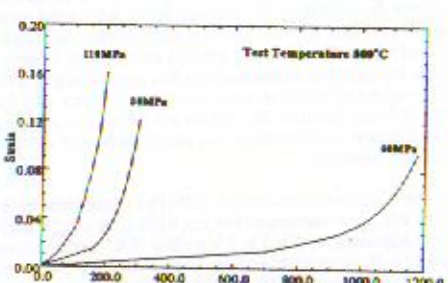

Fig.4 Creep curves for Hastelloy XR.

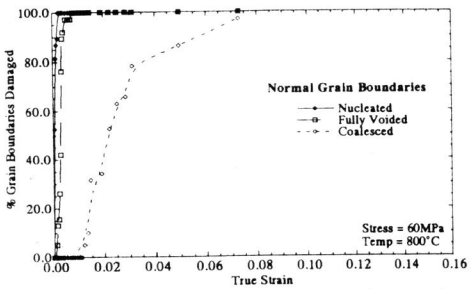

Fig.5a Grain boundary damage as a function of strain for normal boundaries, stress of 60MPa.

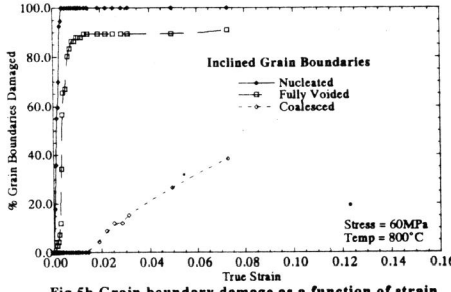

Fig.5b Grain boundary damage as a function of strain for inclined boundaries, stress of 60MPa.

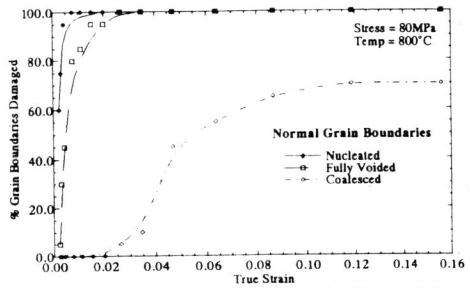

Fig.5c Grain boundary damage as a function of strain

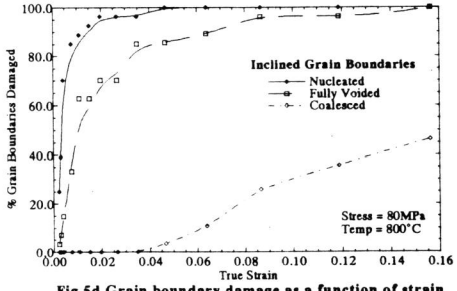

Fig.5d Grain boundary damage as a function of strain for inclined boundaries, stress of 80MPa.

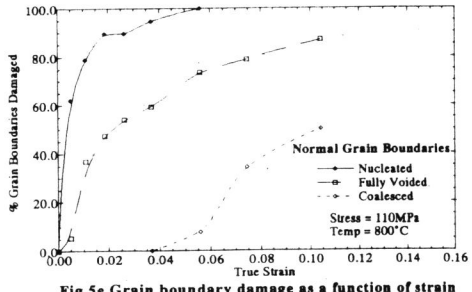

Fig.5e Grain boundary damage as a function of strain for normal boundaries, stress of 110MPa.

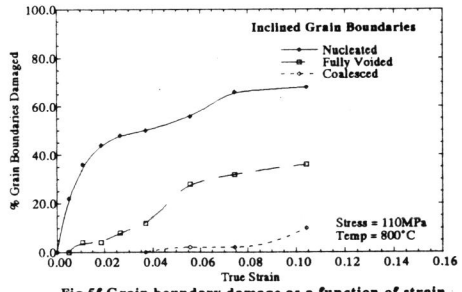

Fig.5f Grain boundary damage as a function of strain for inclined boundaries, stress 110MPa.

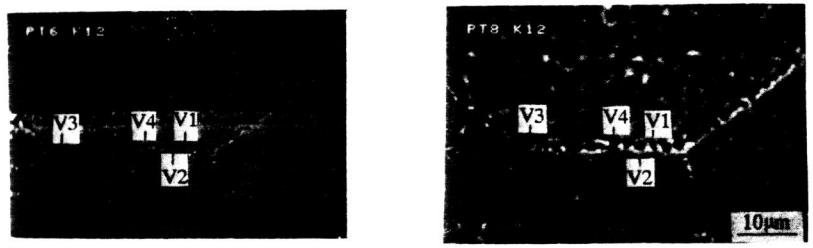

Fig.6 SEM micrographs showing intergranular void development at times of 41.5 and 109h. Stress=80MPa.

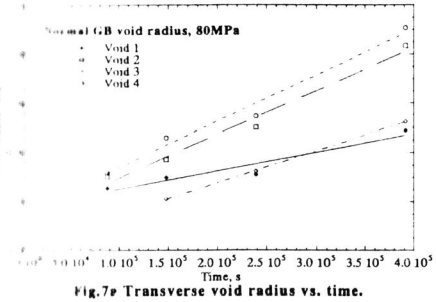

Fig.7a Transverse void radius vs. time.

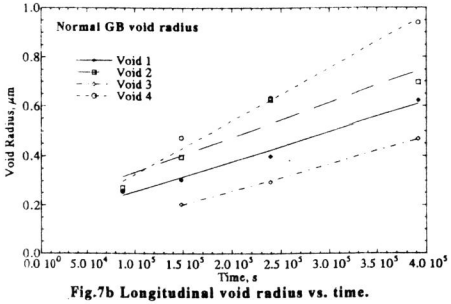

Fig.7b Longitudinal void radius vs. time.

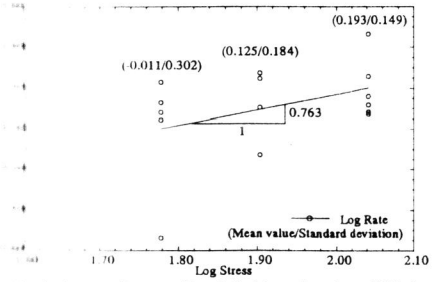

Fig.8a Log cavity growth rate(m/s) vs. log stress(MPa) for transverse void growth.

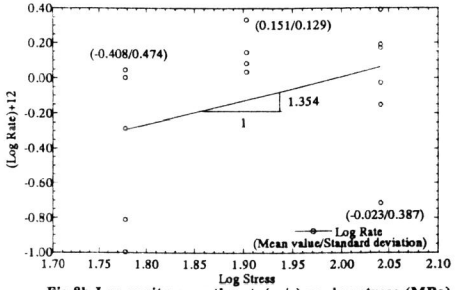

Fig.8b Log cavity growth rate(m/s) vs. log stress (MPa) for tensile void growth.

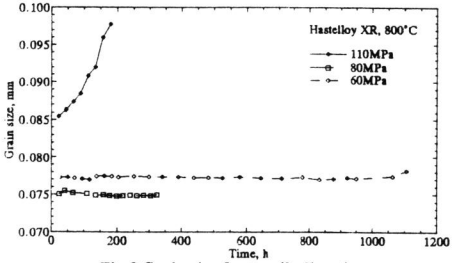

Fig.9 Grain size for tensile direction.